Photoelectron Spectroscopy and Ab Initio Study of the Structure and Bonding of Al_7N^- and Al_7N

Boris B. Averkiev, Seth Call, and Alexander I. Boldyrev*

0300 Old Main Hill, Utah State University, Department of Chemistry and Biochemistry, Logan, Utah 84322-0300

Lei-Ming Wang, Wei Huang, and Lai-Sheng Wang*

Department of Physics, Washington State University, 2710 University Drive, Richland, Washington 99354, and Chemical & Materials Sciences Division, Pacific Northwest National Laboratory, MS K8-88, P.O. Box 999, Richland, Washington 99352

Received: November 5, 2007; In Final Form: January 3, 2008

The electronic and geometrical structures of Al_7N^- are investigated using photoelectron spectroscopy and ab initio calculations. Photoelectron spectra of Al_7N^- have been obtained at three photon energies with six resolved spectral features at 193 nm. The spectral features of Al_7N^- are relatively broad, in particular for the ground state transition, indicating a large geometrical change from the ground state of Al_7N^- to that of Al_7N. The ground state vertical detachment energy is measured to be 2.71 eV, whereas only an upper limit of ~1.9 eV can be estimated for the ground state adiabatic detachment energy due to the broad detachment band. Global minimum searches for A_7N^- and Al_7N are performed using several theoretical methods. Vertical electron detachment energies are calculated using three different methods for the lowest energy structure and compared with the experimental data. Calculated results are in excellent agreement with the experimental data. The global minimum structure of Al_7N^- is found to possess C_{3v} symmetry, which can be viewed as an Al atom capping a face of a N-centered Al_6N octahedron. In the ground state of Al_7N, however, the capping Al atom is pushed inward with the three adjacent Al−Al distances being stretched outward. Thus, even though Al_7N still possesses C_{3v} symmetry, it is better viewed as a N-coordinated by seven Al atoms in a cage-like structure. The chemical bonding in Al_7N^- is discussed on the basis of molecular orbital and natural bond analysis.

1. Introduction

Metal clusters doped with one or more heteroatoms provide a new approach to manipulate the physical and chemical properties of clusters. Doped clusters are interesting chemical species with novel modes of chemical bonding. Understanding the structures and chemical bonding of such clusters may lead to rational designs of structurally and electronically stable clusters for applications in cluster-assembled nanomaterials or catalysis.

Aluminum nitride is an important semiconductor material. However, there have been relatively few experimental and theoretical studies on aluminum nitride clusters.[1−15] Experimentally, it is difficult to produce $(AlN)_x$ type clusters due to the overwhelming thermodynamic stability of the N_2 molecule. In an attempt to produce $(AlN)_x^-$ clusters, Li and Wang were able to observe aluminum clusters doped with only one N atom, Al_xN^-.[10] Photoelectron spectra for a series of Al_xN^- clusters ($x = 2-22$) at 193 nm have been reported and compared to those of pure Al_x^- clusters.[10] The N-doped aluminum clusters are interesting and in larger sizes the Al_xN^- clusters are observed to exhibit similar electronic structures as pure $Al_{(x-1)}^-$ clusters. Recently, we have performed joint photoelectron spectroscopic and ab initio studies on a series of Al_xN^- ($x = 3-6$) clusters to elucidate their electronic and structural evolution as a function of size.[12,13] We have found that the global minimum structures of Al_xN^- ($x = 3-5$) are planar. The 2D to 3D structural transition occurs at $x = 6$. We have shown that Al_6N^- possesses two closely lying low-energy structures, which can be described as Jahn-Teller distortions from the corresponding symmetric D_{3h} and O_h anions of Al_6N^{3-}, respectively.

In the current work, we report a joint photoelectron spectroscopy (PES) and ab initio study on Al_7N^- and its neutral counterpart Al_7N. The neutral Al_7N cluster is an intriguing species because it is valence-isoelectronic to Al_7C^-, which has been reported to be a particularly stable cluster that can be used as a building block for cluster-assembled materials.[16,17] The stability of Al_7C^- has been predicted due to its stable 18-electron shell closing. It would be interesting to compare the structure and bonding between Al_7N and Al_7C^-. There are several previous theoretical studies on the Al_7N cluster.[7−9,14,15] We performed a detailed PES study on Al_7N^- and measured its PES spectra at three photon energies 355, 266, and 193 nm. Extensive calculations have been carried out to search for the global minimum structures for Al_7N^- and Al_7N. The calculated Al_7N^- global minimum structure was confirmed by comparing the calculated vertical detachment energies (VDEs) with the experimental PES spectra. We found that the global minimum of Al_7N^- is a N-centered Al_6N octahedron capped by one Al atom with C_{3v} symmetry. The global minimum structure of Al_7N also has C_{3v} symmetry but undergoes a significant geometry change

* Corresponding authors. E-mail: boldyrev@cc.usu.edu (A.I.B.), ls.wang@pnl.gov (L.S.W.).

10.1021/jp7106236 CCC: $40.75 © 2008 American Chemical Society
Published on Web 01/31/2008

relative to the anion. It can be viewed as a N atom coordinated by seven Al atoms in a cage-like structure, similar to Al_7C^-.

2. Experimental Method

The experiment was performed using a magnetic-bottle PES apparatus with a laser vaporization cluster source; details of the experimental apparatus have been published elsewhere.[18] Briefly, the Al_7N^- clusters were produced by laser vaporization of a disk target compressed from mixed powders of Al and AlN using pure helium as the carrier gas. A 10 cm long and 3 mm diameter extender tubing was used in the cluster source to allow adequate thermerlization of the nascent clusters. This was found to produce relatively cold clusters even under room temperature source conditions, which were important to yield well-resolved PES spectra.[19,20] The anion clusters were extracted from the cluster beam perpendicularly and were analyzed using a time-of-flight mass spectrometer. We showed previously that only Al_xN^- clusters with one N impurity atom could be observed under this condition.[10] The anion clusters of interest were mass-gated and decelerated before being photodetached by a laser beam. Photoelectrons were collected at near 100% collecting efficiency by the magnetic bottle and analyzed in a 3.5 m long electron flight tube. In the current experiment, three photon energies were used for photodetachment, 355 nm (3.496 eV) and 266 nm (4.661 eV) from a Nd:YAG laser and 193 nm (6.424 eV) from an ArF excimer laser. The electron energies were calibrated by the known spectrum of Rh^-. The electron energy resolution ($\Delta Ek/Ek$) was about 2.5%, i.e. ~25 meV for 1 eV electrons.

3. Theoretical Methods

We performed initial computational searches for the global minimum of Al_7N^- and Al_7N using our gradient embedded genetic algorithm (GEGA) program written by Alexandrova[21,22] and our simulated annealing program written by Call. In our simulated annealing Monte Carlo search for the global minimum, we used a population of 20 randomly generated structures at an initial temperature of 10 000 K with an effective Boltzmann constant of 10.0 hartree K^{-1}, which allowed us to have the initial percentage of accepted transitions above 90%. After each iteration the temperature decreased according to $T_n = 0.9995T_{n-1}$. The atomic coordinate perturbation P started at 0.3 Å and decreased according to $P_n = 0.9995^{1/2}P_{n-1}$. The maximum allowed interatomic distance was 3.0 Å. The minimum interatomic distances were 1.7 Å between N and Al and 2.5 Å between Al and Al. The Monte Carlo simulation continued until the percentage of accepted transitions decreased to 10% and the final temperature decreased to 25 K. We used a hybrid method known as B3LYP[23−25] with the small split-valence basis sets (3-21G) for energy, gradient and force calculations, with simulated annealing performing single-point energy calculations and GEGA performing gradient optimizations. We reoptimized geometries and calculated frequencies for the lowest structures using the B3LYP method with the polarized split-valence basis sets (6-311+G*).[26−28] Total energies of the lowest structures were also calculated using the CCSD(T)[29−31] method with the extended 6-311+G(2df) basis sets at the B3LYP/6-311+G* geometries.

The vertical electron detachment energies were calculated using the R(U)CCSD(T)/6-311+G(2df) method, the outer valence Green Function method (R(U)OVGF/6-311+G(2df))[32−36] as well as the time-dependent DFT method[37,38] (TD B3LYP/6-311+G(2df)) all at the B3LYP/6-311+G* geometry. In the last approach, the first vertical electron detachment energies were calculated at the B3LYP level of theory as the lowest transitions from the doublet state of the anion into the final lowest singlet or triplet states of the neutral species. Then the vertical excitation energies in the neutral species (at the TD-B3LYP level) were added to the lowest singlet and triplet VDEs to get the second and higher VDEs. Core electrons were frozen in treating the electron correlation at the R(U)CCSD(T) and R(U)OVGF levels of theory.

The B3LYP, R(U)CCSD(T), and R(U)OVGF calculations were performed using the Gaussian 03 program.[39] Molecular orbital visualization was done using the MOLDEN3.4 program.[40]

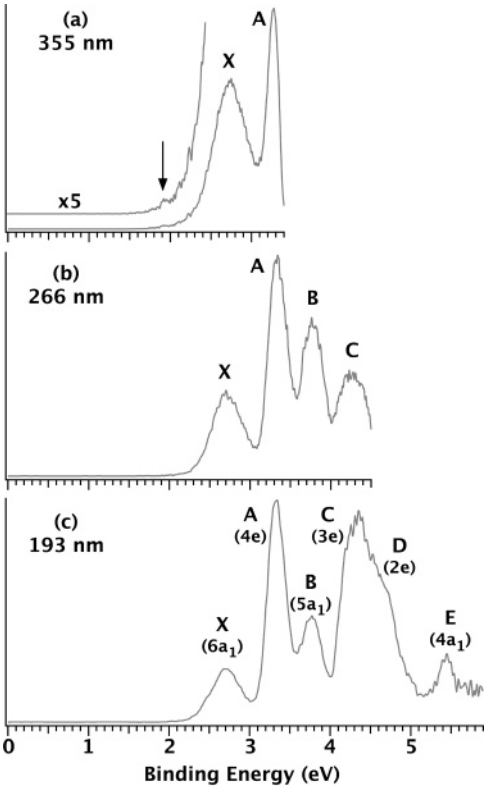

Figure 1. Photoelectron spectra of Al_7N^- at (a) 355 nm (3.496 eV), (b) 266 nm (4.661 eV), and (c) 193 nm (6.424 eV). The molecular orbital origin of each band is labeled in (c) according to theoretical calculations in Table 1 for the global minimum C_{3v} structure.

4. Experimental Results

Figure 1 shows the PES spectra of Al_7N^- at three different photon energies. A total of six distinct detachment bands can be identified in the 193 nm spectrum (Figure 1c), where the C and D bands overlap. All the PES bands seem to be intrinsically broad; i.e., the band widths do not seem to change with photon energies (the instrumental resolution is better at lower photon energies). The apparent sharper band A in the 355 nm spectrum (Figure 1a) is due to a spectral cutoff at ~3.3 eV. The broad spectral widths suggest either a large geometry change upon photodetachment and/or overlapping electronic states. The ground state band X is particularly broad with a long, low-energy tail, making it very difficult to evaluate the adiabatic detachment energy (ADE). This observation implies that there is a major geometry change between the ground state of Al_7N^- and that of neutral Al_7N, meaning that there may be a negligible Franck−Condon factor for the 0−0 transition. We note that there appears to be a step in the low binding energy side in the 355 nm spectrum (see inset of Figure 1a). This step at ~1.9 eV is taken as an upper limit for the ADE for the X band. The VDE

TABLE 1: Experimental Vertical Detachment Energies (VDE) Compared to Calculated VDEs from the Global Minimum Structure I of Al_7N^- at Three Levels of Theory (Energies in eV)

			VDE (theo)		
feature	VDE (exp)	final state and the electronic configuration	TD-B3LYP	OVGF[b]	ΔCCSD(T)
X	2.71 (4)	$^1A_1$, $3a_1^24a_1^22e^43e^45a_1^24e^46a_1^0$	2.56	3.04 (0.87)	2.67
A	3.34 (4)	^3E, $3a_1^24a_1^22e^43e^45a_1^24e^36a_1^1$	3.06	3.24 (0.86)	3.36
		^1E, $3a_1^24a_1^22e^43e^45a_1^24e^36a_1^1$	3.32	*c*	*c*
B	3.77 (4)	$^3A_1$, $3a_1^24a_1^22e^43e^45a_1^14e^46a_1^1$	3.56	3.75 (0.86)	3.69
		$^1A_1$, $3a_1^24a_1^22e^43e^45a_1^14e^46a_1^1$	3.82	*c*	*c*
C	4.35 (5)	^3E, $3a_1^24a_1^22e^43e^35a_1^24e^46a_1^1$	4.19	4.33 (0.85)	*c*
		^1E, $3a_1^24a_1^22e^43e^35a_1^24e^46a_1^1$	4.41	*c*	*c*
D	~4.6	^3E, $3a_1^24a_1^22e^33e^45a_1^24e^46a_1^1$	4.58	4.54 (0.83)	*c*
		^1E, $3a_1^24a_1^22e^33e^45a_1^24e^46a_1^1$	4.81	*c*	*c*
E	5.45 (4)	$^3A_1$, $3a_1^24a_1^12e^43e^45a_1^24e^46a_1^1$	5.40	5.43 (0.81)	*c*

[a] Numbers in parentheses represent the uncertainty in the last digit. [b] Values in parentheses represent the pole strength of the OVGF calculation. [c] This value cannot be calculated at this level of theory.

of the X band is measured to be 2.71 eV. VDEs for all the six PES bands are given in Table 1 and are compared with theoretical calculations.

5. Theoretical Results

Al_7N^-. We initially performed simulated annealing and GEGA searches for the global minimum of Al_7N^- at B3LYP/3-21G level separately for doublet and quartet states. Figure 2 displays the first 11 low-lying doublet structures (I−XI) and the lowest quartet structure (XII) from simulated annealing. These isomers were recalculated at the B3LYP/6-311+G* level for geometry and at CCSD(T)/6-311+G(2df)//B3LYP/6-311+G* level for relative total energies.

The structure I ($^2A_1$, $1a_1^21e^42a_1^23a_1^24a_1^22e^43e^45a_1^24e^46a_1^1$) with C_{3v} symmetry was found by both searches to be the global minimum (Figure 2 and Table 2). It is a face-capped Al_6N octahedron. A similar structure was reported previously by Leskiw et al.,[7] who did not specify the point group symmetry. The Al-capped octahedral structure for Al_7N^- is quite stable; the closest-lying isomer (II) is 10.2 kcal/mol higher at CCSD(T)/6-311+G(2df)//B3LYP/6-311+G* level of theory. This isomer can be described as square-face-capped trigonal prism and is related to the global minimum of Al_6N^-.[13] The lowest quartet structure (XII) is 34.3 kcal/mol (at CCSD(T)/6-311+G(2df)//B3LYP/6-311+G*) higher than the global minimum structure.

Al_7N. As with the anion, we performed simulated annealing and GEGA searches for the global minimum structure of neutral Al_7N at the B3LYP/3-21G level separately for singlet and triplet states. The geometries for all the low-lying structures were then recalculated at B3LYP/6-311+G* level, and relative energies were recalculated at the CCSD(T)/6-311+G(2df)//B3LYP/6-311+G* level. Both searches found structure XIII as the global minimum (Figure 2 and Table 2). The structure XIII ($^1A_1$, $1a_1^21e^42a_1^23a_1^24a_1^22e^43e^45a_1^24e^4$) with C_{3v} symmetry, can be generated from the global minimum of Al_7N^- by removing one electron from the singly occupied HOMO. Even though they have the same point group symmetry, there is a significant structural change from the global minimum of Al_7N^- to that of neutral Al_7N. In the ground state of Al_7N, the capping Al atom is pushed inward with the three adjacent Al−Al distances being stretched outward. Thus, neutral Al_7N can be viewed as a N atom coordinated by the seven Al atoms in a cage-like structure, whereas in Al_7N^- the N atom is only coordinated by six Al atom, and the capping atom is in the second coordination shell. A similar Al_7N structure was obtained previously by several authors.[7−9,14,15] It can be seen from Figure 2 that the global minimum structure of Al_7N is highly stable and that all the alternative structures (XIV−XX) are significantly higher in energy.

6. Comparison between the Calculated VDEs and Experiment and Interpretations of the Experimental PES Spectra

Our extensive structural search for Al_7N^- did not locate any isomers close in energy to the global minimum; the closest isomer is 10.2 kcal/mol higher at UCCSD(T)/6-311+G(2df)//B3LYP/6-311+G* (Figure 2). Therefore, only the global minimum structure should be responsible for the photoelectron spectra. Indeed, the experimental PES spectra exhibit no hints of the presence of another isomer, which sometimes gives weak features in the low-binding energy side.[41] The calculated VDEs for the global minimum structure I of Al_7N^- at the TD-B3LYP/6-311+G(2df), UOVGF/6-311+G(2df) and CCSD(T)/6-311+G(2df) levels of theory are compared with the experimental data in Table 1.

Ground State PES Band X. The ground state of Al_7N^- is a doublet ($^2A_1$) with an electron configuration of $1a_1^21e^42a_1^23a_1^24a_1^22e^43e^45a_1^24e^46a_1^1$. According to our calculation the first PES band (X) of Al_7N^- corresponds to removal of the electron from the singly occupied $6a_1$ orbital. The calculated VDE for this detachment channel is 2.67 eV at the UCCSD(T)/6-311+G(2df) level of theory, 3.04 eV at the UOVGF/6-311+G(2df) level of theory, and 2.56 eV at the TD-B3LYP/6-311+G(2df) level of theory (Table 1). The pole strength in the UOVGF calculation was found to be 0.87, indicating that the detachment channel can be primarily described by a one-electron detachment process. The UCCSD(T) result is in excellent agreement with the experimental VDE of 2.71 eV (Table 1). Surprisingly, the VDE at UOVGF/6-311+G(2df) is significantly overestimated (by 0.33 eV) compared to the experimental value, whereas TD-B3LYP underestimated the VDE by 0.15 eV.

The calculated ADE for the ground state transition is 1.86 eV at UCCSD(T)/6-311+G(2df), which is significantly smaller than the VDE (2.67 eV) at the same level of theory. The large relaxation energy (VDE − ADE) of 0.81 eV reflects the large geometry change between the ground states of the anion and the neutral structure; this is in good agreement with the observed broad ground state PES band (X). The calculated ADE at 1.86 eV is in excellent agreement with the estimated upper limit of 1.9 eV from the 355 nm PES spectrum, indicating that there is a finite Franck−Condon factor for the 0−0 transition and that the 1.9 eV value may be taken as representing the true ADE or the electron affinity for neutral Al_7N.

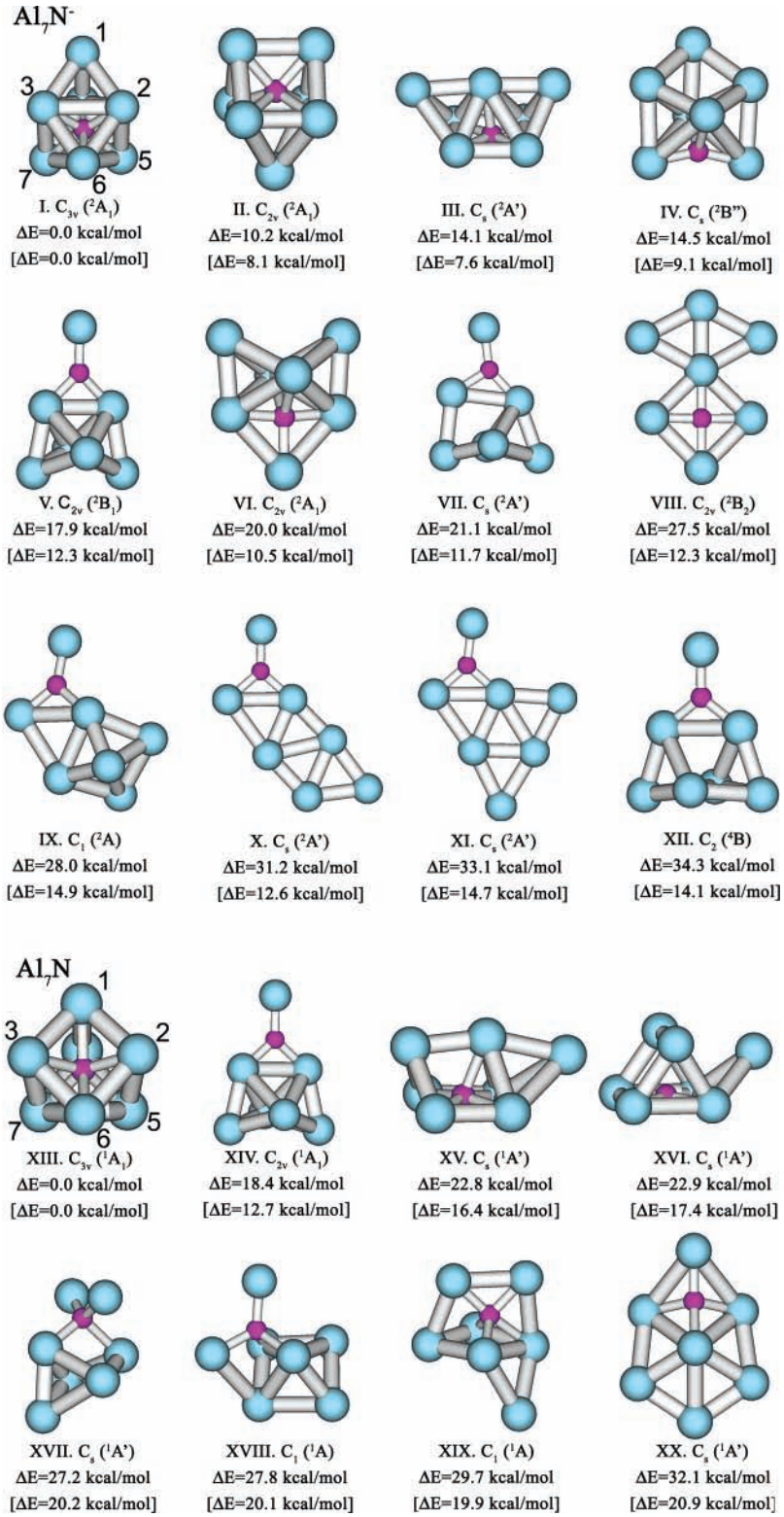

Figure 2. Computationally found low-lying isomers for Al_7N^- and Al_7N. Relative energies are given at CCSD(T)/6-311+G(2df)//B3LYP/6-311+G* and at B3LYP/6-311+G* in brackets.

Higher Binding Energy Detachment Bands (A to E). Because of the ground state of Al_7N^- is open shell with a single electron occupying the $6a_1$ HOMO, detachment from any other fully occupied orbitals results in triplet and singlet final states, as shown in Table 1. Unfortunately, the singlet excited states cannot be calculated using the OVGF or the CCSD(T) methods. The TD-B3LYP method yields triplet-singlet splittings ranging from 0.22 to 0.26 eV (Table 1). The second detachment channel is from the HOMO-1 4e orbital. The calculated VDE to the ^3E final state is 3.36 eV at CCST(T) level, which is in excellent agreement with the measured VDE of the A band at 3.34 eV. The OVGF VDE for this channel is 3.24 eV, which is in reasonable agreement with the experimental value. TD-B3LYP appears to underestimate this VDE by ~0.3 eV. Because of the broad spectral width (i.e., Franck−Condon envelope) associated with the anion to neutral geometry change, as well as the expected Jahn−Teller effect for the ^3E final state, the transition to the singlet state cannot be resolved in the current

TABLE 2: Molecular Properties of the Al_7N, Al_7N^-, and Al_7N^{2-} Species Calculated at B3LYP/6-311+G*

	Al_7N, XIII, C_{3v} ($^1A_1$)	Al_7N^-, I, C_{3v} ($^2A_1$)	Al_7N^{2-}, C_{3v} ($^1A_1$)
E, au	−1752.0019598	−1752.0661946	−1752.0192342
$R(N-Al_1)$, Å	2.137	3.003	3.515
$R(N-Al_2)$, Å	2.106	1.986	1.996
$R(N-Al_5)$, Å	2.123	2.074	2.041
$R(Al_1-Al_2)$, Å	2.613	2.722	2.840
$R(Al_2-Al_3)$, Å	3.540	3.045	2.794
$R(Al_2-Al_5)$, Å	2.649	2.742	2.840
$R(Al_5-Al_6)$, Å	2.811	2.918	2.943
ω_1 (a_1), cm^{-1}	490 (291)[a]	511 (158)[a]	535 (225)[a]
ω_2 (a_1), cm^{-1}	343 (1)	357 (5)	364 (16)
ω_3 (a_1), cm^{-1}	287 (14)	280 (0)	272 (4)
ω_4 (a_1), cm^{-1}	232 (1)	188 (5)	226 (60)
ω_5 (a_1), cm^{-1}	116 (1)	162 (9)	150 (3)
ω_6 (a_2), cm^{-1}	201 (0)	131 (0)	94 (0)
ω_7 (e), cm^{-1}	488 (260)	553 (173)	532 (163)
ω_8 (e), cm^{-1}	297 (2)	253 (5)	238 (2)
ω_9 (e), cm^{-1}	259 (7)	223 (0)	232 (0)
ω_{10} (e), cm^{-1}	226 (15)	193 (4)	159 (29)
ω_{11} (e), cm^{-1}	166 (0)	146 (22)	118 (12)
ω_{12} (e), cm^{-1}	51 (0)	63 (1)	73 (0)

[a] Values in parentheses represent relative absorbance intensities in the IR spectrum (km/mol).

PES spectra even under the slightly higher resolution at 266 nm (Figure 1b). In addition, the intensity for the singlet detachment channel is expected to be lower than the triplet channel, and it is likely to be buried on the higher binding energy side of the A band. This appears to be the case for all the higher energy detachment channels (B to E), where the singlet states are not explicitly resolved.

The next detachment channel is from the nondegenerate HOMO-2 $5a_1$ orbital. The calculated VDEs from both CCSD-(T) (3.69 eV) and OVGF (3.75 eV) are in excellent agreement with the experimental VDE of the B band at 3.77 eV. TD-B3LYP again underestimates the VDE for this detachment channel by ~0.2 eV. The relatively lower intensity of the B band is consistent with the nondegenerate nature of the $5a_1$ orbital.

The next two detachment channels are from the degenerate HOMO-3 3e and HOMO-4 2e orbitals, which should correspond to the C and D bands, respectively. The calculated VDEs for these two channels at OVDF are 4.33 and 4.54 eV, which are fairly close to each other. The calculated data are again in excellent agreement with the experimental PES spectra, in which the C and D bands overlap (Figure 1c). The final detachment channel comes from the HOMO-5 $4a_1$ orbital, corresponding to the E band. Surprisingly, both TD-B3LYP (5.40 eV) and OVGF (5.43 eV) yield VDEs, which are in excellent agreement with the experimental value of 5.45 eV. The $4a_1$ orbital is nondegenerate, again consistent with the relatively weak intensity of the E band.

The overall agreement between the theoretical results and the experimental data is truly excellent, leaving no ambiguity about the C_{3v} global minimum structure (I, Figure 2) for Al_7N^-. It is also interesting to note that the single particle MO picture works extremely well for Al_7N^-; there is a precise one-to-one correspondence between the MOs and the observed PES bands, as labeled in Figure 1c. The pole strengths in the OVGF calculations for all the detachment channels are >0.80, which also provides good indications for the validity for the single particle MO picture for the detachment processes from Al_7N^-. We have found previously that OVGF works well for Al-based clusters.[12,13,42−56] However, in the current case, the first VDE was severely overestimated by OVGF, although the overall spectral pattern predicted by OVGF is in excellent agreement with experiment, especially for the high binding energy features. Although slightly less accurate, the TD-B3LYP method also yields a quite good spectral pattern in comparison with experiment. In particular, the ability to compute both triplet and singlet final states is a distinct advantage of the TD−DFT method. The CCSD(T) method is the most accurate, but it can only be used to calculate the first three detachment channels. Therefore, the combination of the three theoretical methods is very powerful, providing a quantitative interpretation of the PES spectra of Al_7N^- and unequivocally establishing its global minimum structure.

7. Chemical Bonding in Al_7N and Al_7N^-

The Al_7N neutral cluster is isoelectronic to the so-called "magic" cluster Al_7C^-, which is quite prominent in the Al_nC^- mass spectra.[17] Both Al_7N and Al_7C^- have similar global minimum structures, and we expect that Al_7N should also be a very stable cluster. Enhanced stability of Al_7C^- has already been discussed in the literature.[15,17,57] Initially Leskiw and Castleman[57] suggested that the stability of Al_7C^- could be reconciled within a jellium model framework where Al_7C^- could be viewed as a compound jellium cluster formed from Al_6 with a closed shell of 18 electrons and an AlC^- unit. However, this bonding picture does not agree with the global minimum structure of Al_7C^- because the C atom is located inside the Al_7 cage and one cannot identify an AlC unit. Thus, it seems that the stability of Al_7C^- is more complicated than the jellium model predicts. Indeed, the total number of valence electrons in Al_7C^- is 26, and according to the jellium model, one should have the following electronic configuration $1s^21p^61d^{10}2s^21f^6$, which is not a closed-shell system and should not have any special stability. Later on, Reveles et al.[17] proposed an alternative explanation, in which the closed-shell $1s^21p^61d^{10}2s^22p^6$ electronic configuration is used instead of $1s^21p^61d^{10}2s^21f^6$. The earlier appearance of the 2p subshell instead of the 1f subshell was explained on the basis of the higher stability of the $2s^22p^6$ subshell. Sun et al.[15] explained the "magic" behavior of Al_7C^- on the basis of a large HOMO−LUMO gap. However, we can better understand the structure and bonding in the Al_7N^- anion using an alternative interpretation based on the stability of the highly stable octahedral Al_6N^{3-} unit, which we used to understand the structure and bonding in Al_6N^-.[13]

The ground electronic state of Al_7N^- is a doublet $^2A_1$ with an electron configuration of $1a_1^21e^42a_1^23a_1^24a_1^22e^43e^45a_1^24e^46a_1^1$. To simplify our chemical bonding analysis, we fill up the singly occupied HOMO in Al_7N^- by one more electron. The geometry of the resulting Al_7N^{2-} structure was reoptimized at the B3LYP/6-311+G* level of theory (Figure 3a and Table 2). The final geometry of the structure of Al_7N^{2-} is very similar to the optimized structure I of Al_7N^- (Figure 2). From a purely geometrical perspective, one can formally view the structure of Al_7N^{2-} as a salt between an octahedral Al_6N^{3-} anion and a face-capping Al^+ cation. The octahedral structure and chemical bonding in the Al_6N^{3-} anion were discussed in detail previously.[13] Even though an isolated Al_6N^{3-} triply charged anion is not electronically stable, it has a repulsive Coulomb barrier on the electron ejection pathway[58−60] and therefore it has a finite lifetime at the optimized O_h geometry.

Before discussing the chemical bonding in Al_7N^{2-}, let us briefly review the chemical bonding in Al_6N^{3-}, which is closed shell ($^1A_{1g}$) with an electron configuration of $1a_{1g}^21t_{1u}^62a_{1g}^2\ 2t_{1u}^61e_g^41t_{2g}^6$.[13] The lowest valence MO $1a_{1g}$ is primarily the 2s-AO of the central nitrogen atom. The next triply degenerate $1t_{1u}$ MO can be assigned to three $2p_x$-, $2p_y$-, and

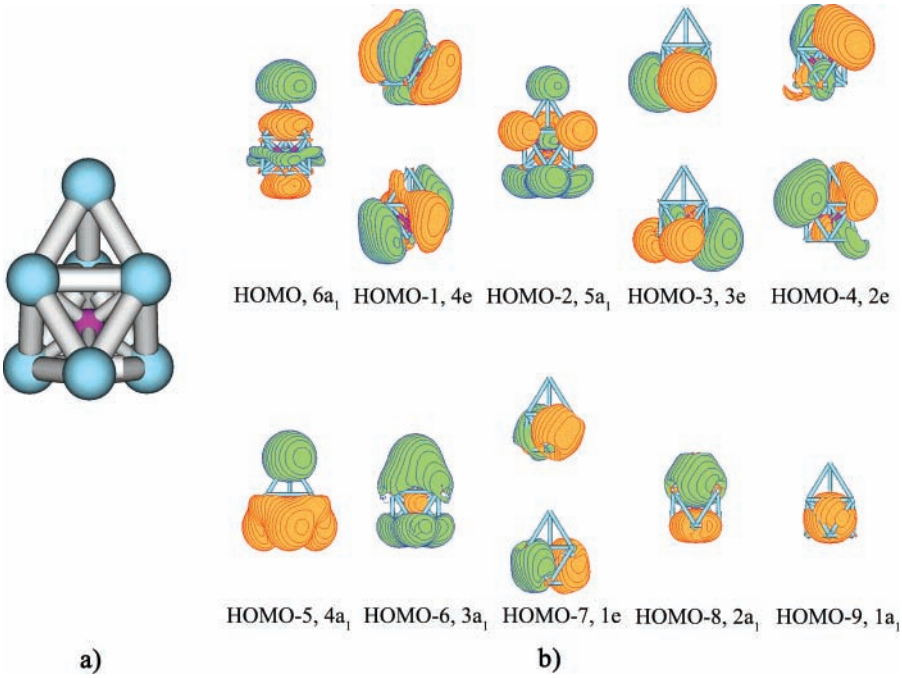

Figure 3. Optimized structure (a) and molecular orbital pictures (b) for Al_7N^{2-} calculated at B3LYP/6-311+G*.

$2p_z$-AOs of the central N atom. The next six valence MOs ($2a_{1g}$, $2t_{1u}$, and $1e_g$) are primarily formed by the 3s-AOs of the aluminum atoms and they can be viewed as six lone pairs located on the Al atoms. Finally, the completely bonding and triply degenerate $1t_{2g}$-HOMO is formed by the tangential 3p-AOs of the Al atoms, and it is responsible for the delocalized tangential bonding between the Al atoms. To test our interpretation of the bonding in Al_6N^{3-}, we performed NBO analysis of the Al_6N^{3+} cation (at the geometry of Al_6N^{3-}), in which the delocalized $1t_{2g}$-HOMO was empty. The NBO analysis reveals four lone pairs of N with occupation numbers on the order of 1.95 |e| (2s) and 1.98 |e| (2p), and one lone pair at every Al with the occupation number of 1.75 |e| (99.5% composed of 3s-AOs). Thus, in O_h Al_6N^{3-} the chemical bonding can be approximately described as the central atom carrying an effective charge -3 (N^{3-}), which is ionically bonded to an octahedral Al_6 cluster, with every Al carrying a lone pair. The $1t_{2g}$-HOMO is the only orbital responsible for delocalized Al−Al bonding and tangential aromaticity. The Al_6 cluster keeps its octahedral structure in Al_6N^{3-}, because N^{3-} can fit perfectly in the cavity of the octahedron and because the closed shell N^{3-} unit substitutes a completely bonding pair of electrons in the $2a_{1g}$-MO in Al_6^{2-}.[56]

All valence MOs of the Al_7N^{2-} anion are presented in Figure 3b. The HOMO ($6a_1$) and HOMO−1 (4e) are responsible for the delocalized bonding, as in the case with $1t_{2g}$-HOMO in Al_6N^{3-}. To understand bonding in the Al_7N^{2-} anion, we performed an analogous NBO analysis for the putative Al_7N^{4+} cation at the geometry of the Al_7N^{2-} anion, but with the $6a_1$-HOMO and 4e-HOMO−1 empty. The NBO analysis of Al_7N^{4+} revealed four lone pairs of N with occupation numbers from 1.90 |e| to 1.97 |e| and one lone pair at every Al with the occupation number from 1.57 |e| (97.6% composed of 3s-AOs) to 1.64 |e| (99.4% composed of 3s-AOs). On the basis of this analysis, we conclude that indeed there is a formal building block in the Al_7N^{2-} cluster $\{Al^+[Al_6N^{3-}]\}$, though the bonding between Al^+ and Al_6N^{3-} is more covalent than ionic. One can see in Figure 3b that the 3p-AOs of the capping Al atom participate in the delocalized bonding between the aluminum atoms. The question now is, could the building block Al_6N^{3-} be a part of the larger doped Al_xN^- clusters, and could it even be a part of a N-doped solid aluminum? These questions are worth pursuing in future studies of larger Al_xN^- clusters.

8. Summary

The Al_7N^- cluster has been investigated by a combined photoelectron spectroscopy and ab initio study. Well-resolved, albeit broad, spectral features were used to compare with the calculated VDEs. The global minimum structures of Al_7N and Al_7N^- were located using both a genetic algorithm and simulated annealing. The structure of Al_7N^- is found to possess C_{3v} symmetry, which can be viewed as an Al capping an octahedron Al_6N unit. In the neutral Al_7N, significant geometry relaxation is observed, consistent with the broad PES spectral features. The calculated VDEs for the C_{3v} Al_7N^- global minimum structure are in excellent agreement with the PES spectra. The structure and chemical bonding of Al_7N^- are understood using the closed-shell Al_7N^{2-}, which possesses similar C_{3v} structure as Al_7N^-. Al_7N^{2-} can be viewed as an Al^+ capping the face of a highly stable octahedral Al_6N^{3-} building block. The stability of the octahedral Al_6N^{3-} was used previously to understand the structures of Al_6N an Al_6N^-.[13] It would be interesting to discover if the N-centered Al_6N^{3-} octahedron is a building block in larger Al_xN^- clusters.

Acknowledgment. The theoretical work done at Utah State University was supported by the National Science Foundation (CHE-0404937). Computer time from the Center for High Performance Computing at Utah State University is gratefully acknowledged. The computational resource, the Uinta cluster supercomputer, was provided through the National Science Foundation under Grant CTS-0321170 with matching funds provided by Utah State University. The experimental work done at Washington State University was supported by the National Science Foundation (DMR-0503383) and was performed at the W. R. Wiley Environmental Molecular Sciences Laboratory, a national scientific user facility sponsored by DOE's Office of Biological and Environmental Research and located at Pacific Northwest National Laboratory, which is operated for DOE by Battelle.

References and Notes

(1) Schleyer, P. v. R.; Boldyrev, A. I. *J. Chem. Soc., Chem. Commun*. **1991**, 1536.

(2) Zakrzewski, V. G.; Niessen, W. v.; Boldyrev, A. I.; Schleyer, P. v. R. *Chem. Phys.* **1993**, *174*, 167.

(3) Nayak, S. K.; Khana, S. N.; Jena, P. *Phys. Rev. B* **1998**, *57*, 3787.

(4) Nayak, S. K.; Rao, B. K.; Jena, P.; Li, X.; Wang, L. S. *Chem. Phys. Lett*. **1999**, *301*, 379.

(5) Boo, B. H.; Liu, Z. *J. Phys. Chem*. *A* **1999**, *103*, 1250.

(6) Andrews, L.; Zhou, M.; Chertihin, G. V.; Bare, W. D.; Hannachi, Y. *J. Phys. A* **2000**, *104*, 1656.

(7) Leskiw, B. R.; Castleman, A. W., Jr. Ashman, C.; Khanna, S. N. *J. Chem. Phys.* **2001**, *114*, 1165.

(8) Ling, L.; Song, B.; Cao, P.-L. *J. Mol. Struct. (THEOCHEM*) **2005**, *728*, 215.

(9) Gou, L.; Wu, H.-S. *Int. J. Quantum Chem*. **2006**, *106*, 1250.

(10) Li, X.; Wang, L. S. *Eur. Phys. J. D* **2005**, *34*, 9.

(11) Meloni, G.; Sheehan, S. M.; Parsons, B. F.; Neumark, D. M. *J. Phys. Chem. A* **2006**, *110*, 3527.

(12) Averkiev, B. B.; Boldyrev, A. I.; Li, X.; Wang, L. S. *J. Chem. Phys.* **2006**, *125*, 124305.

(13) Averkiev, B. B.; Boldyrev, A. I.; Li, X.; Wang, L. S. *J. Phys. Chem. A* **2007**, *111*, 34.

(14) Wang, B.; Shi, D.; Chen, X.; Wang, G.; Zhao, J. *Int. J. Modern Phys. B* **2005**, *19*, 2380.

(15) Sun, Q.; Wang, Q.; Gong, X. G.; Kumar, V.; Kawazoe, Y. *Eur. Phys. J. D* **2002**, *18*, 77.

(16) Aschman, C.; Khanna, S. N.; Pederson, M. R.; Kortus, J. *Phys. Rev. B* **2000**, *62*, 16956.

(17) Reveles, J. U.; Khanna, S. N.; Roach, P. J.; Castleman, A. W., Jr. *Proc. Natl. Acad. Sci*. (*U.S.A.*) **2006**, *103*, 18405.

(18) Wang, L. S.; Cheng, H. S.; Fan, J. *J. Chem. Phys*. **1995**, *102*, 9480.

(19) Li, X.; Wu, H.; Wang, X. B.; Wang, L. S. *Phys. Rev. Lett*. **1998**, *81*, 1909.

(20) Akola, J.; Manninen, M.; Hakkinen, H.; Landman, U.; Li, X.; Wang, L. S. *Phys. Rev. B* **1999**, *60*, R11297.

(21) Alexandrova, A. N.; Boldyrev, A. I.; Fu, Y-J.; Wang, X. B.; Wang, L. S. *J. Chem. Phys.* **2004**, *121*, 5709.

(22) Alexandrova, A. N.; Boldyrev, A. I. *J. Chem. Theory Comput.* **2005**, *1*, 566.

(23) Becke, A. D. *J. Chem. Phys.* **1993**, *98*, 5648.

(24) Vosko, S. H.; Wilk, L.; Nusair, M. *Can. J. Phys.* **1980**, *58*, 1200.

(25) Lee, C.; Yang, W.; Parr, R. G. *Phys. Rev. B* **1988**, *37*, 785.

(26) (a) Binkley, J. S.; Pople, J. A.; Hehre, W. J. *J. Am. Chem. Soc.* **1980**, *102*, 939. (b) Gordon, M. S.; Binkley, J. S.; Pople, J. A.; Pietro, W. J.; Hehre, W. J. *J. Am. Chem. Soc.* **1982**, *104*, 2797. (c) Pietro, W. J.; Francl, M. M.; Hehre, W. J.; Defrees, D. J.; Pople, J. A.; Binkley, J. S. *J. Am. Chem. Soc.* **1982**, *104*, 5039.

(27) McLean, A. D.; Chandler, G. S. *J. Chem. Phys.* **1980**, *72*, 5639.

(28) Clark, T.; Chandrasekhar, J.; Spitznagel, G. W.; Schleyer, P. v. R. *J. Comput. Chem.* **1983**, *4*, 294.

(29) Cizek, J. *Adv. Chem. Phys.* **1969**, *14*, 35.

(30) Knowles, P. J.; Hampel, C.; Werner, H.-J. *J. Chem. Phys.* **1993**, *99*, 5219.

(31) Raghavachari, K.; Trucks, G. W.; Pople, J. A.; Head-Gordon, M. *Chem. Phys. Lett.* **1989**, *157*, 479.

(32) Cederbaum, L. S. *J. Phys. B* **1975**, *8*, 290.

(33) (a) Ortiz, J. V. *Int. J. Quantum Chem., Quantum Chem. Symp*. **1989**, *23*, 321. (b) Lin, J. S.; Ortiz, J. V. *Chem. Phys. Lett*. **1990**, *171*, 197.

(34) Zakrzewski, V. G.; Ortiz, J. V.; Nichols, J. A.; Heryadi, D.; Yeager, D. L.; Golab, J. T. *Int. J. Quantum Chem.* **1996**, *60*, 29.

(35) Dahnovsky, Y. *J. Chem. Phys*. **2007**, *126*, 234111.

(36) Kletsov, A.; Dahnovsky, Y. *Phys. Rev. B* **2007**, *76*, 035304.

(37) Bauernshmitt, R.; Alrichs, R. *Chem. Phys. Lett.* **1996**, *256*, 454.

(38) Casida, M. E.; Jamorski, C.; Casida, K. C.; Salahub, D. R. *J. Chem. Phys.* **1998**, *108*, 4439.

(39) Frisch, M. J.; Trucks, G. W.; Schlegel, H. B.; Scuseria, G. E.; Robb, M. A.; Cheeseman, J. R.; Montgomery, J. A., Jr.; Vreven, T.; Kudin, K. N.; Burant, J. C.; Millam, J. M.; Iyengar, S. S.; Tomasi, J.; Barone, V.; Mennucci, B.; Cossi, M.; Scalmani, G.; Rega, N.; Petersson, G. A.; Nakatsuji, H.; Hada, M.; Ehara, M.; Toyota, K.; Fukuda, R.; Hasegawa, J.; Ishida, M.; Nakajima, T.; Honda, Y.; Kitao, O.; Nakai, H.; Klene, M.; Li, X.; Knox, J. E.; Hratchian, H. P.; Cross, J. B.; Bakken, V.; Adamo, C.; Jaramillo, J.; Gomperts, R.; Stratmann, R. E.; Yazyev, O.; Austin, A. J.; Cammi, R.; Pomelli, C.; Ochterski, J. W.; Ayala, P. Y.; Morokuma, K.; Voth, G. A.; Salvador, P.; Dannenberg, J. J.; Zakrzewski, V. G.; Dapprich, S.; Daniels, A. D.; Strain, M. C.; Farkas, O.; Malick, D. K.; Rabuck, A. D.; Raghavachari, K.; Foresman, J. B.; Ortiz, J. V.; Cui, Q.; Baboul, A. G.; Clifford, S.; Cioslowski, J.; Stefanov, B. B.; Liu, G.; Liashenko, A.; Piskorz, P.; Komaromi, I.; Martin, R. L.; Fox, D. J.; Keith, T.; Al-Laham, M. A.; Peng, C. Y.; Nanayakkara, A.; Challacombe, M.; Gill, P. M. W.; Johnson, B.; Chen, W.; Wong, M. W.; Gonzalez, C.; Pople, J. A. *Gaussian 03*, revision D.01; Gaussian, Inc.: Wallingford, CT, 2004

(40) MOLDEN3.4. Schaftenaar, G. MOLDEN3.4, CAOS/CAMM Center, The Netherlands, 1998.

(41) Zhai, H. J.; Kiran, B.; Li, J.; Wang, L. S. *Nat. Mater*. **2003**, *2*, 827.

(42) Boldyrev, A. I.; Simons, J.; Li, X.; Chen, W.; Wang, L. S. *J. Chem. Phys*. **1999**, *110*, 8980.

(43) Li, X.; Wang, L. S.; Boldyrev, A. I.; Simons, J. *J. Am. Chem. Soc*. **1999**, *121*, 6033.

(44) Boldyrev, A. I.; Simons, J.; Li, X.; Wang, L. S. *J. Chem. Phys*. **1999**, *111*, 4993.

(45) Boldyrev, A. I.; Simons, J.; Li, X.; Wang, L. S. *J. Am. Chem. Soc*. **1999**, *121*, 10193.

(46) Boldyrev, A. I.; Li, X.; Wang, L. S. *J. Phys. Chem. A* **2000**, *104*, 5358.

(47) Cannon, N. A.; Boldyrev, A. I.; Li, X.; Wang, L. S. *J. Chem. Phys*. **2000**, *113*, 2671.

(48) Wang, L. S.; Boldyrev, A. I.; Li, X.; Simons, J. *J. Am. Chem. Soc*. **2000**, *122*, 7681.

(49) Boldyrev, A. I.; Li, X.; Wang, L. S. *Angew. Chem., Int. Ed*. **2000**, *39*, 3307.

(50) Geske, G. D.; Boldyrev, A. I.; Li, X.; Wang, L. S. *J. Chem. Phys*. **2000**, *113*, 5130.

(51) Li, X.; Zhang, H. F.; Wang, L. S.; Geske, G. D.; Boldyrev, A. I. *Angew. Chem., Int. Ed*. **2000**, *39*, 3630.

(52) Li, X.; Kuznetsov, A. E.; Zhang, H. F.; Boldyrev, A. I.; Wang, L. S. *Science* **2001**, *291*, 859.

(53) Li, X.; Zhang, H. F.; Wang, L. S.; Kuznetsov, A. E.; Cannon, N. A.; Boldyrev, A. I. *Angew. Chem., Int. Ed*. **2001**, *40*, 1867.

(54) Li, X.; Wang, L. S.; Cannon, N. A.; Boldyrev, A. I. *J. Chem. Phys*. **2002**, *116*, 1330.

(55) Kuznetsov, A. E.; Birch, K. A.; Boldyrev, A. I.; Li, X.; Zhai, H. J.; Wang, L. S. *Science* **2003**, *300*, 622.

(56) Kuznetsov, A. E.; Boldyrev, A. I.; Zhai, H. J.; Li, X.; Wang, L. S. *J. Am. Chem. Soc*. **2002**, *124*, 11791.

(57) Leskiw, B. D.; Castleman, A. W., Jr. *Chem. Phys. Lett*. **2000**, *316*, 31.

(58) Wang, X. B.; Ding, C. F.; Wang, L. S. *Phys. Rev. Lett*. **1998**, *81*, 3351.

(59) Wang, L. S.; Ding, C. F.; Wang, X. B.; Nicholas, J. B. *Phys. Rev. Lett.* **1998**, *81*, 2667.

(60) Wang, X. B.; Wang, L. S. *Nature* **1999**, *400*, 245.